Flows of cohesive granular media

Sandip Mandal[1], *Adrien* Gans[1], *Maxime* Nicolas[1], and *Olivier* Pouliquen[1,*]

[1]Aix Marseille Univ, CNRS, IUSTI UMR7343, Marseille, France

Abstract. Cohesive granular media have broad applications in industries. However, our understanding of their flow behavior is still limited compared to dry granular media, although rich knowledge about their static and plastic properties has been gained. In this paper, we provide some insights into the flow behavior of cohesive granular media from our recent numerical studies using an inclined plane and a plane shear cell. We evidence that the cohesive nature of flows is significantly affected by material properties of the particles like stiffness and inelasticity in addition to the inter-particle adhesion and introduce the concept of "effective" adhesion, which incorporates the effects of these three variables. We propose constitutive relations involving dimensionless inertial number and "effective" cohesion number, based on the "effective" adhesion to describe the rheology. We also show that increasing adhesion increases the hysteresis in granular media, evidencing the existence of a prominent shear weakening branch in the friction coefficient *versus* inertial number rheological curve. Moreover, we reveal that this increasing hysteresis gives rise to the increasing occurrence of shear banding instability, pointing to the increasing possibility of jamming in cohesive granular media. Finally, we present a promising experimental approach to investigate the flow behavior of cohesive granular materials, based on a simple method of preparing a long time stable medium with a controlled adhesion between particles.

1 Introduction

Many materials used in industries exist in powder form and often face enormous problems during storage, handling, or flowing. These difficulties stem from adhesion forces between the grains, which create a bulk cohesion for the granular medium, inducing blockage and agglomeration phenomena. Empirical characterization of the "flowability" of powders is carried out in industries based on a series of measurements ranging from compaction properties to heap angle [1, 2]. However, the physical basis of the concept of "flowability" is unclear. Cohesive granular media are also involved in many geophysical events like landslides, sediment transport, etc. Therefore, cohesive granular media have been a subject of numerous numerical and experimental studies—while most of them focus on quasi-static properties of the material using triaxial or shear cell configurations, only a few concern its flow properties and rheology.

In the absence of adhesion, the rheology of granular media (which we will call dry granular media in the following) is relatively well-described by a frictional viscoplastic framework [3–6] and two empirical constitutive laws: the coefficient of friction $\mu(I)$ and the volume fraction $\phi(I)$ as a function of the dimensionless inertial number I. A granular medium, consisting of grains of size d and density ρ_p, sheared under a confining normal stress σ_{zz} at a shear rate $\dot{\gamma}$, experiences a shear stress $\tau = \mu(I)\sigma_{zz}$, and its volume fraction evolves as $\phi = \phi(I)$, where $I = \dot{\gamma}d/\sqrt{\sigma_{zz}/\rho_s}$. This simple approach proved to be sufficient for describing many observations [7–9], albeit limited to dense flow regimes between dilute flows, for which kinetic theories are more appropriate [10], and quasi-static flows, in which more complex effects such as non-local cooperativity effects must be taken into account [11, 12].

When an adhesion between the grains exists, the rheology is modified. The presence of a new stress scale given by the adhesion force implies that the inertial number is no longer the only dimensionless number controlling the dynamics. If the adhesion is characterized by the detachment force N_c required to detach two bonded grains in the absence of any other external forces, another dimensionless number called the cohesion number can be defined as $C = N_c/\sigma_{zz}d^2$ [13, 14], which compares the detachment force to the typical force that a grain undergoes due to the confining normal stress. The friction coefficient and the volume fraction then become functions of the inertial number and the cohesion number: $\mu = \mu(I, C)$ and $\phi = \phi(I, C)$. Some numerical studies [13, 14] using a simple JKR-like [15], yet non-hysteretic adhesion force model and others [16, 17] using capillary adhesion force model have verified these scaling and reported that $\mu(I, C)$ and $\phi(I, C)$ increases and decreases, respectively, with increasing I and C. A new set of scaling laws involving a generalized inertial number has also been proposed [18, 19].

Employing the simple adhesive force model as in Ref. [13, 14] in discrete numerical simulations, we examine the flows down an inclined plane and in a plane shear cell. We provide new insights into the rheology of cohesive granular materials from these studies in Section 2. One main result concerns the role of stiffness and in-

*e-mail: olivier.pouliquen@univ-amu.fr

A video is available at https://doi.org/10.48448/zsev-jh63

elasticity of the particles in cohesive granular flows [20]. These material properties are known to have no influence on the rheology of dry granular media unless their values are very small. However, they play a dramatic role in the cohesive case—for the same adhesion, softer and/or more dissipative grains yield a more cohesive macroscopic behavior. The introduction of the concept of an "effective" adhesion, taking into account the effects of adhesion, stiffness, and inelasticity, rationalizes the observations. The other important result concerns the low inertial number limit of the rheology. We show that the adhesion introduces a more prominent shear weakening branch in the rheological curve, where the friction coefficient decreases when increasing the inertial number. We exhibit that the existence of this branch in the rheological curve has strong consequences for the stability of the flow—a more prominent shear banding occurs for the cohesive grains.

Although the above numerical studies provided some understanding of the flow behavior of cohesive granular media, there are only little insights from experiments. While most experiments deal with the determination of quasi-static properties [21], using triaxial shear testers or shear cells, only a few concerned the flow properties and the rheology [17, 22]. From an experimental point of view, the difficulty lies in the control of the inter-particle adhesive forces. It would indeed be interesting to have a material in which it would be possible to control the cohesion at will, making it possible to continuously study the transition from a non-cohesive granular medium for which the rheological laws are relatively well established, to a cohesive medium. The addition of a liquid to a granular medium is one of the commonly used methods in the literature for producing a cohesive medium—the quantity of liquid controls the intensity of capillary interaction, which in turn determines the macroscopic cohesion of the material [17, 23, 24]. However, the dynamics of unsaturated granular media is complex, with phenomena like liquid migration and merging of the capillary bridges [17, 25]. In Section 3 of this paper, we describe a recipe to create a model cohesive granular medium by coating the grains with a thin polymer layer. With this protocol we obtain a material with a desired adhesion and which is extremely stable over time, allowing for extensive studies on cohesive flows.

2 New insights into the rheology of cohesive granular materials from Discrete Element Method (DEM) simulations

DEM simulation is a very powerful tool for studying granular flows. One can investigate the role of the interaction forces, from the simplest to the most realistic ones, and vary at will the parameters of the grain properties like elasticity, friction, or adhesion, which is not possible experimentally. It also provides a direct way to analyze the link between the microscopic behavior at the grain scale and the macroscopic bulk rheology. Here we investigate the influence of an adhesion force on the rheology in two configurations: flow down an inclined plane and flow in a plane shear cell.

2.1 Simulation method

The simulated material is made of frictional, inelastic, cohesive spherical grains, which have an average size d with a polydispersity of 20% and an average mass m. The details of the inter-particle contact forces are given in [20] and the numerical code used is the one developed in [26]. The normal contact force between two grains comprises three contributions: a linear elastic part $\boldsymbol{N}_{ij}^{el} = -k_n\delta$ proportional to the overlap between the particles δ, k_n being the stiffness; a viscous force $\boldsymbol{N}_{ij}^{vis} = -\gamma_n m_{eff}\boldsymbol{c}_{ij}^{\boldsymbol{n}}$, where $\boldsymbol{c}_{ij}^{\boldsymbol{n}}$ is the normal relative velocity, $m_{eff} = m_i m_j/(m_i + m_j)$ is the effective mass, and γ_n is the normal damping coefficient (in the following, we introduce the quality factor $Q = \sqrt{k_n/m}/\gamma_n$, which quantifies the level of dissipation of the particles and is directly related to the inelastic restitution coefficient in absence of adhesion, the higher the Q, the lesser the dissipation); an adhesive force [13] $\boldsymbol{N}_{ij}^{ad} = \sqrt{4k_n N_c\delta}$, where N_c is the minimum pull-off force to separate two particles (equal to the minimum of the sum of the elastic and adhesive forces). Note that the adhesive interaction model is short-range, meaning that the force vanishes when two grains are not in contact, unlike in wet capillary bridges. The tangential contact force comprises an elastic force $\boldsymbol{T}_{ij}^{el} = -k_t s$, with $k_t = 2/7k_n$ and s is the relative tangential overlap from the beginning of a contact. It is set to $\boldsymbol{T}_{ij} = \mu_p(\boldsymbol{N}_{ij}^{el} + \boldsymbol{N}_{ij}^{vis})$, where μ_p is the inter-particle friction coefficient when sliding occurs.

2.2 Flows on an inclined plane: effect of the stiffness and the dissipation on the cohesive nature of the flow

We first analyze the flow of the cohesive granular material down a rough plane inclined at an angle θ from horizontal. The rough base (shown in red in Fig. 1a) comprises a random packed bed of the same grains of height $1.8d$. The simulation box has length $L_x = 20d$, width $L_y = 20d$, and height $L_z = 40d$. Periodic boundary conditions are applied in the x and y directions. In the case of cohesionless granular material, the velocity profile is given by the well-known Bagnold profile [27], with a shear distributed all across the layer, and a velocity increasing with a power 3/2 with the height. When adhesion is introduced, the velocity profile is modified. A plug region with no shear appears at the top of the layer, due to the existence of a cohesive yield stress induced by the adhesion. Keeping the inclination constant, the higher the adhesion between the grains, the larger the plug regions, and the slower the flow as evidenced in Fig. 1b and observed in previous studies [13, 28]. Ultimately when adhesion is strong enough, the flow stops.

A surprising result arises when varying the stiffness k_n and the dissipation of the particles through the quality factor Q. While k_n and Q play no major role in the dense flows of cohesionless grains [27, 29], we observe here that they dramatically modify the flow when adhesion is present [30, 31]. Increasing the stiffness decreases the

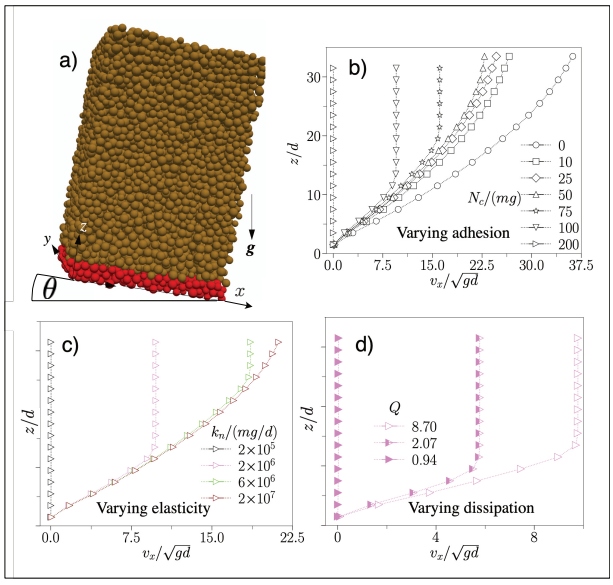

Figure 1. Flow down an inclined plane: (a) sketch of the simulated configuration; velocity profiles for (b) different adhesion N_c; (c) different stiffness k_n; (c) different quality factor Q.

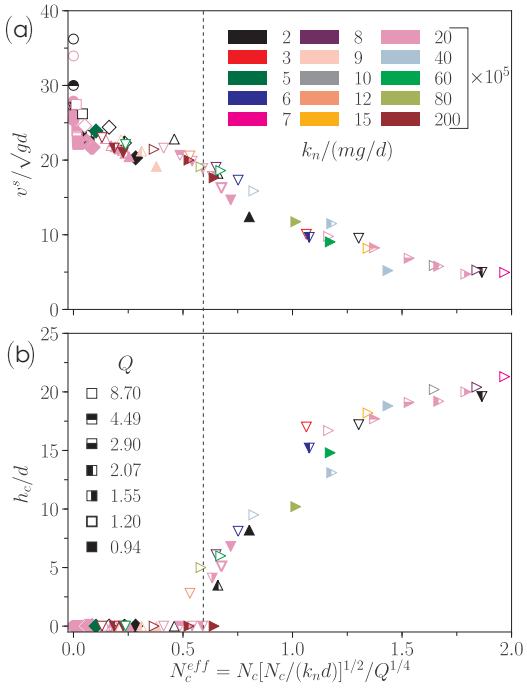

Figure 2. (a) Free surface velocity v_s and (b) thickness h_c of the plug region as a function of the effective adhesion force (eq.1) for different values of the adhesion N_c, stiffness k_n and quality factor Q, showing the collapse of all the data.

plug flow, up to a point where the plug region disappears for stiff enough particles (Fig. 1c). Although in a less dramatic way, decreasing the quality factor also increases the plug region (Fig. 1c). Decreasing the stiffness or increasing the dissipation plays the same role as increasing the adhesion. This result shows that in a cohesive granular material, the cohesive nature of the flow does not only depend on the adhesion force between the grains but also on the other contact properties of the grains.

To go one step further in the description of the cohesive properties of the flow, we introduce the notion of a dynamic "effective" adhesive force N_c^{eff}, and we seek for an expression as a function of $\frac{N_c}{k_n d}$ the modified Bond Number introduced by Gu et al [32] and the quality factor:

$$N_c^{eff} = N_c \left[\left(\frac{N_c}{k_n d} \right)^{\alpha} \frac{1}{Q^{\beta}} \right], \qquad (1)$$

where α and β are constants. The idea behind this scaling is to check if the influence of adhesion, stiffness, and dissipation can be embedded in a single parameter N_c^{eff}, acting as an "effective" adhesive force in dynamic conditions. To test this idea, we performed a series of simulations at a fixed angle but different values of N_c, k_n and Q. From the computed velocity profiles, we extract for each simulation the free surface velocity v_s and the thickness of the plug region h_c, the two main characteristics of the flow. We then seek for the best values of α and β in Eq. 1, such that v_s and h_c obtained from all the runs collapse when plotted as a function of N_c^{eff} given by Eq. 1. Figure 2 shows that with $\alpha = 1/2$ and $\beta = 1/4$, the collapse is good, meaning that in the range of parameters investigated, the flow is indeed controlled solely by the "effective" adhesive force N_c^{eff}.

The interpretation of this scaling is not straightforward. However, the existence of an interplay between the inter-particle adhesion and the mechanical properties of the grains can be evidenced considering the dynamics of a binary collision. For a given impact velocity, two particles may remain attached together if N_c is large but also if k_n or Q are small [33]. As mentioned in [34], this suggests that energy arguments should be taken into account when analyzing the influence of adhesion in granular flows.

From a rheological perspective, the evidence of an "effective" adhesion force controlling the flow, suggests us to introduce an "effective" cohesion number $C^{eff} = N_c^{eff}/\sigma_{zz} d^2$ by analogy with the cohesion number introduced in [13], and to seek for constitutive laws in the form of a friction law $\mu(C^{eff}, I)$, and volume fraction $\phi(C^{eff}, I)$. In the inclined plane configuration, the stress being non-uniform, inferring the rheology is not simple [20]. We then switch to the plane shear configuration to study in detail the constitutive laws.

2.3 Plane shear cell: shear banding and evidence of a shear weakening branch

The three-dimensional plane shear cell, depicted in Fig.3a, comprises two rough walls of area $20d \times 20d$. The height varies from $H = 8d$ to $H = 34d$. Periodic boundary conditions are imposed in longitudinal x and lateral y directions. A normal stress σ_{zz} is applied to the top plate, which is free to move vertically but moves horizontally with a prescribed velocity U. A typical run consists in increasing continuously U to explore a range of imposed shear rate U/H and measuring the shear stress τ that applies on the

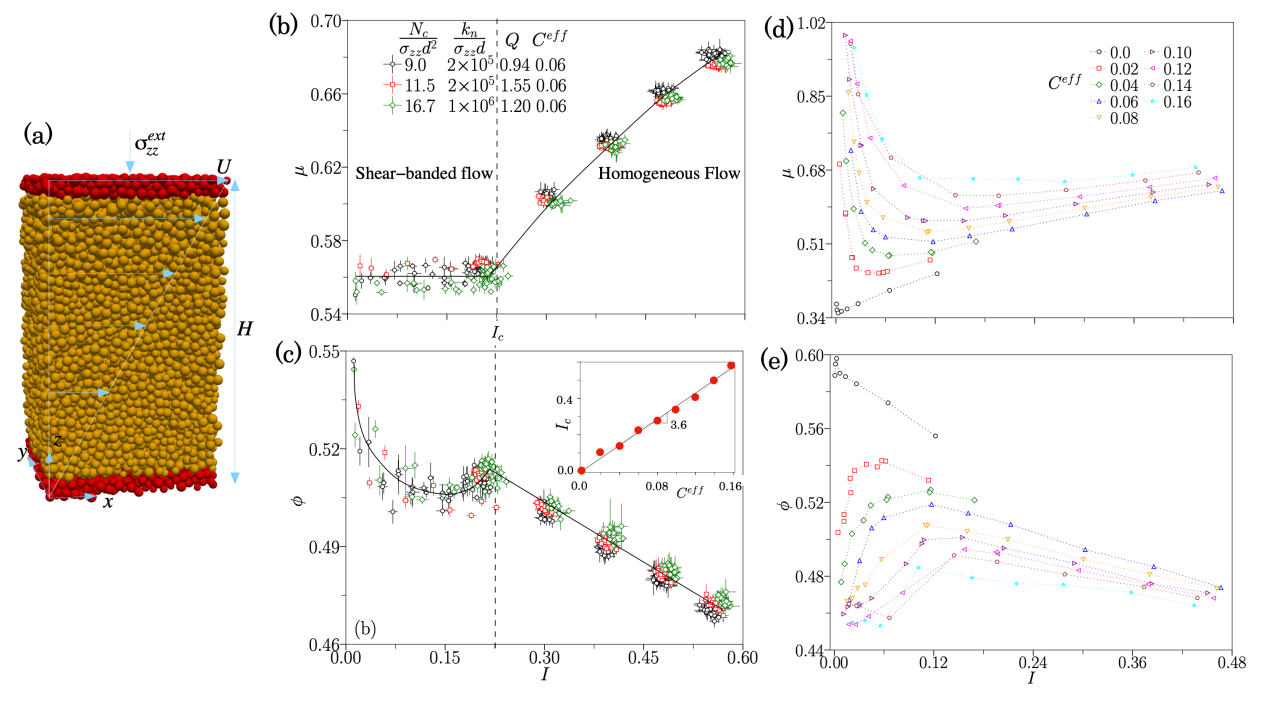

Figure 3. Plane shear cell: (a) sketch of the simulated configuration; (b) friction coefficient and (c) volume fraction as function of the inertial number I for various particle parameters keeping the "effective" cohesion number the same $C^{eff} = 0.06$, for a large system $H = 34d$. Inset: I_c delimiting the occurence of shear banding as a function of C^{eff}. (d) friction coefficient μ and (e) volume fraction ϕ as a function of I in a small system $H = 8d$ for which the flow remains uniform, for different cohesion number C^{eff}.

top plate (hence the friction coefficient $\mu = \tau/\sigma_{zz}$), as well as the volume fraction ϕ.

Typical constitutive laws measured in the large system ($H = 34d$) are plotted in Figs. 3 (b) and (c) for the friction coefficient μ and the volume fraction ϕ as a function of the inertial number I for three different sets of particle parameters, the adhesion, stiffness, and quality factor. The first observation is that similarly to the inclined plane, the data for different adhesion, stiffness, and dissipation can be collapsed if they are chosen such that the "effective" cohesion number based on the "effective" adhesion force defined in Eq. 1 is constant. However, we notice that a better collapse is obtained if the power β is taken equal to 0.7 instead of 0.25 found in the inclined plane, α being unchanged equal to 0.5. The second important observation is that two different behaviors are evident. Above a critical inertial number I_c denoted by the dashed line, the material is uniformly sheared across the cell, and the friction coefficient increases (resp. the volume fraction decreases) when increasing I, typical trends reported in [13, 14, 16, 17]. Below I_c, we observe that the flows become inhomogenous, with the development of a shear band similar to what is observed in other complex fluids [35, 36]. In this regime, the measured friction coefficient shows a plateau and the volume fraction, a non-monotonic variation when changing I. The range of inertial number where shear banding occurs increases when increasing the "effective" cohesion number as shown in the inset of Fig. 3c.

When studying more precisely the domain of existence of shear banding, several peculiar features are observed. First, the location of the shear band varies depending on the initial conditions—it can be either at the top, bottom, or even localized in between the two plates. However, the local shear rate remains the same in all three cases. Secondly, hysteresis exists when increasing and decreasing the inertial number. There exists a range of inertial number close to I_c where both a linear or a shear-banded profile can be obtained depending on the protocol. Lastly, shear banding disappears for small enough systems. For $H = 8d$, the velocity profile remains linear whatever the imposed shear rate. This last property gives access to the intrinsic rheological curves, measuring how the friction coefficient and the volume fraction vary over the whole range of inertial number, keeping the shear rate uniform in the cell (Figs. 3d and e). For a given cohesion number, both curves are strikingly non-monotonic, exhibiting a strong shear-weakening behavior: μ decreases (resp. ϕ increases), with increasing I, reaches a minimum (resp. a maximum), before increasing again (resp. decreasing) following the usual shear-strengthening behavior. The shear weakening branch covers a wider range of inertial number when increasing the cohesion. The existence of such shear weakening rheological branch is commonly assumed to give rise to flow heterogeneities and explains the occurrence of shear banding [36–38]. One important difference between our studied material and other glassy systems where shear banding is observed [39–41] is that the rheology is studied here under confining pressure, not under constant volume fraction. The existence of a shear weakening branch may have dramatic consequences in terms

of the ability of cohesive materials to flow and may be of importance to determine the flowability.

2.4 How cohesion influences the hysteresis between starting and stopping flow conditions

The above simulations were carried out imposing the velocity of the top plate to capture the flow curve. To investigate the starting and stopping properties of cohesive granular flows, we also perform simulations imposing a shear stress on the top plate. Starting from an initially static layer of grains confined between the two plates, the shear stress is slowly increased, up to the point when a flow starts, giving a measure of the starting friction coefficient μ_{PS}^{start}. The shear stress is then slowly decreased until the flow stops, providing a measure of the stopping friction coefficient μ_{PS}^{stop}. Similar measurements are carried out for the inclined plane (IP) configuration, by successively increasing the inclination to trigger the flow and decreasing back the slope to stop the flow, providing the measurements of μ_{IP}^{start} and μ_{IP}^{stop}.

Results are presented in Fig. 4. A first important result concerns the role of the stiffness and dissipation on these quantities. The starting properties are found to depend only on the adhesion force N_c and not on the stiffness k_n and quality factor Q. This shows that the static properties are indeed controlled only by the force necessary to detach two particles. The coefficient μ_{PS}^{start} and μ_{IP}^{start} are thus functions of the cohesion number C. The friction coefficients are found to vary linearly with C (Fig.4a): $\mu_{IP,PS}^{start} = \mu_0 + A_{IP,PS}C$. The friction coefficient being the ratio of the shear stress $\tau_{IP,PS}^{start}$ to the normal stress σ_{zz}, one can show by multiplying this linear relation by σ_{zz}, that it is equivalent to a cohesive Mohr-Coulomb criterion : $\tau_{IP,PS}^{start} = \mu_0\sigma_{zz} + \tau_{IP,PS}^{c}$, μ_0 being the cohesionless friction coefficient, and $\tau_{IP,PS}^{c} = A_{IP,PS}C\sigma_{zz}$ being the cohesive stress, which by definition of C is proportional to $N_c d^2$, a classical estimate of the cohesive stress. By contrast, the stopping friction coefficients (μ_{PS}^{stop}, μ_{IP}^{stop}), being dynamical quantities, not only depend on the adhesion but also on the stiffness and dissipation, and are indeed found to be functions of only the effective cohesion number C^{eff}, not C (Fig.4b). However, the measured values differ between the two configurations: the starting friction coefficient is higher in the inclined plane than in the plane shear, except for the cohesionless case, for which the two values are identical. The opposite is observed for the stopping friction coefficients, where $\mu_{IP}^{stop} < \mu_{PS}^{stop}$. It is not clear why flow initiation and flow cessation occur at different stress levels in the two configurations. One difference lies in the stress distribution, shear stress being homogeneous in the plane shear, whereas it is higher at the bottom in the inclined plane. This may be a sign that other phenomena like fluctuations and/or non-local effects [11] might play a role. An important remark is that the hysteresis disappear if the inter-particle friction is switched to zero, which is reminiscent of what has been observed in granular suspensions [42].

3 Controlling cohesion in experiments

One difficulty in studying cohesive material is the control of the cohesion forces between the particles. Whereas in numerical studies, simplified interaction laws might be introduced in DEM approaches to simulated cohesive grains [43] as we did in the previous sections, experimentally, the control of the cohesion is more challenging. Working with actual powders faces many difficulties, mainly because of a lack of the control on the particle properties. Most of the recent experimental works on cohesive granular materials have focused on capillary cohesion, studying the properties of an assembly of beads mixed with a small amount of a viscous liquid. Here we present a method to prepare a controlled-cohesion granular material (CCGM) made of polyborosiloxane (PBS) coated glass particles, which suits many of the requirements to achieve experiments with a controlled cohesion. The main interest of the method is that the cohesion force between particles can be easily tuned through the PBS coating, and that the obtained material is very stable over long time.

3.1 A method to make a cohesion controlled granular material

The recipe to prepare the cohesion controlled granular material is described in details in [44]. The idea is to coat silica particles with a polyborosiloxane layer (PBS), obtained from polydemethulsiloxane (PDMS) cross linked with boric acid [45, 46]. The protocol is very easy and take place in a heating mixer, where the solution of acid boric, the PDMS and the glass beads are mixed and heated at 110 °C during 90 min to ensure the evaporation of the water. Once cooled, the controlled-cohesion granular material is ready to use. The control parameter is the relative amount of PDMS introduced in the mixture compare to the amount of grains, which fixes the thickness of coating layer b, and thus the adhesion force between the particles. An example of a packing of 3mm coated glass beads is shown in Fig. 5a. To characterize the properties of the cohesive medium obtain using this recipe, we have performed both microscopic and macroscopic measurements.

At the grain scale, we first measured the force necessary to detached two particles and its dependence with the averaged thickness b of the coating layer, computed as the volume of PDMS introduced in the mixture divided by the total surface of the grains. The detachment force F_c between two particles in contact is measured by pulling on one particle, the second one being fixed, and by monitoring the force until detachment occurs. We first study the role of the history of the contact and have shown that the detachment force is independent of the pre-compression imposed to the two adhesive particles in contact. It is also independent of the number of successive contacts. The coating layer thus seems to be robust and remains identical after detachment. However, an influence of the age of the contact has been observed. The adhesion force increases by a factor of two when the waiting time before the measurement goes from zero to 10 minutes. It remains constant for longer time. We also investigate how the detachment force varies with the particle diameter. For the

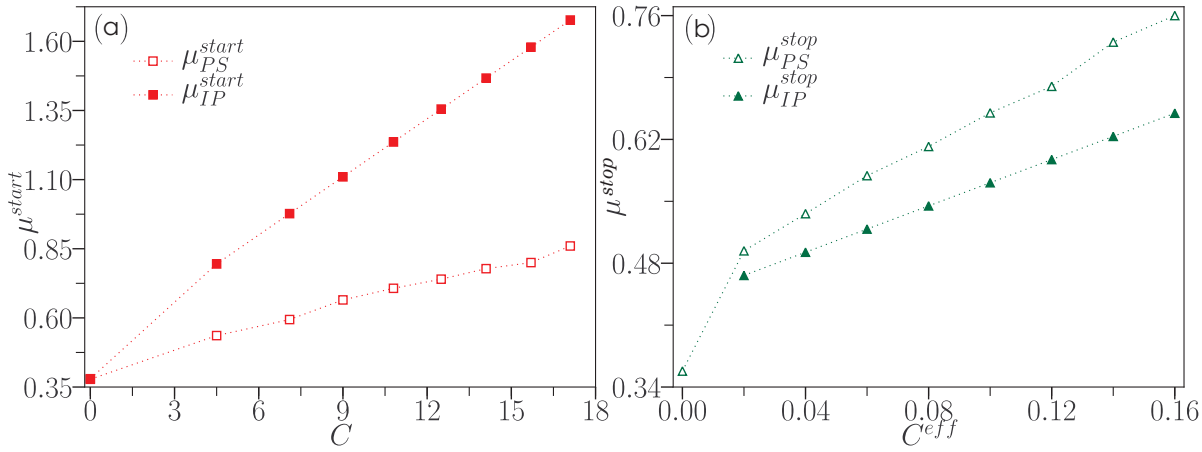

Figure 4. (a) Starting friction coefficient as a function of the cohesion number C and (b) stopping friction coefficient as a function of the effective cohesion number C^{eff} for both the inclined plane (IP) and plane shear (PS) configurations.

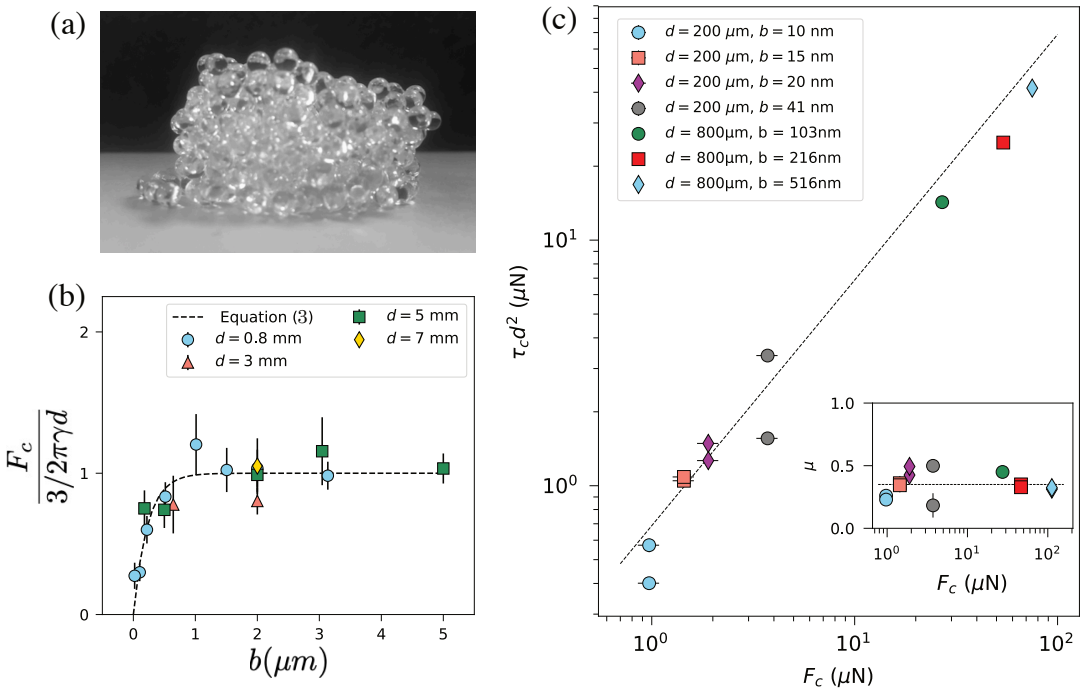

Figure 5. (a) Example of a cohesion-controlled granular material: a pile of glass beads $d = 3$mm with a PBS coating layer of thickness $b = 2.2\mu$m;(b) Adhesion force between two particles normalized by the capillary scaling eq. 2 as a function of the averaged coating thickness b; (c) Cohesive stress times the particle diameter $\tau_c d^2$ as a function of the adhesion force F_c, τ_c being deduced from measurements of the starting angle on an inclined plane.

same waiting time, the adhesion force varies linearly with the diameter. This linear variation is compatible with the simple interpretation of the adhesion force in terms of a capillary force :

$$F_c = g(b)\frac{3}{2}\gamma d \tag{2}$$

where $g(b)$ is a dimensionless function of the averaged coating thickness b. The best fit is obtained for a surface tension $\gamma \approx 24$ mN.m^{-1}, a relevant order of magnitude for the PDMS. In Figure 5b we have plotted the estimate of $g(b)$ from the measurements obtained for different particle diameters and different coating thicknesses for a waiting time of ten seconds. The collapse is good and we can suggest an empirical expression to predict the adhesion force as a function of the coating thickness

$$g(b) = 1 - e^{-b/B}, \tag{3}$$

where $B \approx 230$ nm is a characteristic thickness, which may be related to the particle roughness.

Once the adhesion at the grains scale had been characterized, we have carried out macroscopic experiments to estimate the cohesive stress of the bulk material. To do

so, an inclined plane device has been used and the starting angle at which a uniform layer of material of thickness h starts to flow has been measured for different thicknesses h. According to a simple Mohr Coulomb criterium, flow starts when the shear stress τ at the bottom of the layer reaches a critical value $\tau = \tau_c + \mu_c\sigma$, where σ is the normal stress at the bottom of the layer, τ_c is the cohesive stress and μ_c the friction coefficient. At the bottom of the layer, we have $\tau = \rho g h \sin\theta$ and $\sigma = \rho g h \cos\theta$. We can then plot τ as a function of σ when the critical starting angle is reached for each h, and fit the data by a linear function to estimate τ_c and μ_c. The results for different particle diameters and different coating are plotted in Fig. 6c. As expected from dimensional analysis τ_c scales as the adhesion force divided by the particle diameter F_c/d^2.

The last important result concerns the remarquable stability of the controlled cohesion granular material. Same experiments carried out few months after the preparation of the material provide the same results. The PBS-coated grains seems to be stable for months and large batches can then be prepared before performing large-scale experiments. It also seems to be unaffected by the moisture content of the ambient air since our experiments were performed without humidity control across different temperature and humidity conditions over a year.

3.2 Two examples of cohesive granular flows

The cohesion controlled granular material designed in the previous section can now be used to perform systematic experiments and to bridge the gap between cohesionless granular materials and cohesive ones by increasing progressively the coating thickness. We are currently performing such experiments and only show in this paper preliminary results obtained in two systems. The first one shown in Fig. 6a consists in pouring the material on top of a disk to create sand piles. The three pictures show the final pile obtained for three different coating thicknesses, showing that the slope angle increases with the adhesion force as expected and already reported in many experiments using mixture of grains and viscous liquid [47–49].

The second experiments presented in Fig 6b is the famous dam break experiment. A granular material initially confined in a box is suddenly released by rapidly opening a door. The pile collapses, flows and finally stops and forms a deposit. This configuration has been extensively studied in dry granular media and can serve as a benchmark to study the influence of cohesion. The presence of cohesion modifies the dynamics of the flow in several aspects. The first influence is that the runout decreases when increasing the cohesion. Secondly the morphology of the deposit present an undeformed wedge, which is transported with the landslide and do not participate to the runout. Finally, we have observed that the typical velocity of the flow are affected by the cohesion. These fews experiments shows that the ability to control the cohesion in a stable and easy to handle material open new avenues for experimentally investigating the properties of cohesive granular flows.

4 Conclusion

In this paper, we have presented some new insights into the rheology of cohesive granular media. A first result is that the adhesion force N_c is not the only parameter to be considered when characterizing the "flowability" of the material. While static properties like the onset of the flow is indeed controlled by N_c, when flow occurs, the rheology is also influenced by the stiffness and dissipative nature of the particles, contrary to what we know for dry granular materials. We have shown that this influence can be rationalized by a dynamic "effective" adhesive force, which combines the effects of all the contact parameters in a single quantity. As a consequence, this means that measuring the adhesion force between grains is not sufficient to predict the cohesive properties of the flow of materials. A second major result reported in this paper is the existence of a strong hysteresis in cohesive granular media, with the existence of a shear weakening branch in the rheological curve, i.e., a regime where the friction coefficient decreases when increasing the inertial number. This may have strong implications for applications, as it is a source of instability and of shear localization, which may stop the flow. Lastly, we have presented promising experimental techniques to develop a cohesion controlled granular material. Being able to adjust the adhesion at will in a material opens new perspectives to experimentally investigate the rheology of cohesive granular media.

Acknowledgement

This work was supported by the ANR grant, ANR-17-CE08-0017 under COPRINT (Cohesive Powders Rheology: Innovative Tools) project. The experiments on the dam break were performed in collaboration with Alban Sauret, and took place in his laboratory in the Mechanical Engineering department, UC Santa Barbara.

References

[1] M.V. Antequera, A.M. Ruiz, M.M. Perales, N.M.M. noz, M.J.C. Ballesteros, Int. J. Phar. **103**, 155 (1994)
[2] D. Geldart, E.C. Abdullah, A. Hassanpour, L.C. Nwoke, I. Wouters, China Part. **4**, 104 (2006)
[3] G. MiDi, Eur. Phys. J E **14**, 341 (2004)
[4] F. da Cruz, S. Emam, M. Prochnow, J.N. Roux, F. Chevoir, Phys. Rev. E **72**, 021309 (2005)
[5] P. Jop, Y. Forterre, O. Pouliquen, Nature **441**, 727 (2006)
[6] B. Andreotti, Y. Forterre, O. Pouliquen, *Granular media between fluid and solid* (Cambridge University Press, 2013)
[7] Y. Forterre, J. Fluid Mech. **563**, 123 (2006)
[8] L. Staron, P.Y. Lagrée, S. Popinet, Eur. Phys. J E **37**, 5 (2014)
[9] P.Y. Lagrée, L. Staron, S. Popinet, J. Fluid Mech. **686**, 378 (2011)
[10] I. Goldhirsch, Annu. Rev. Fluid Mech. **35**, 267 (2003)

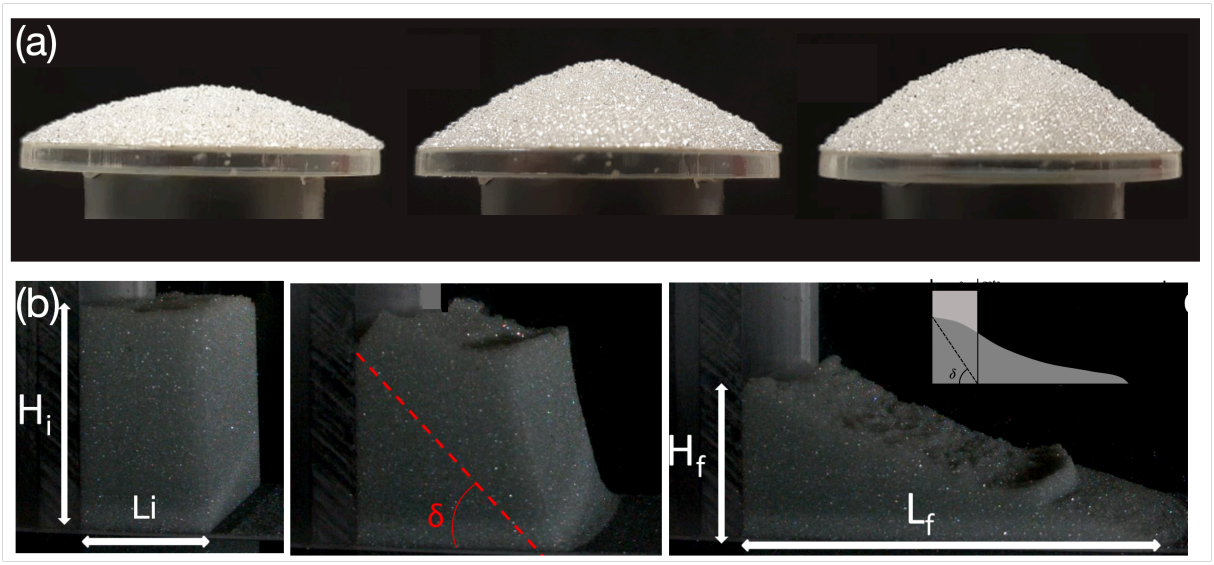

Figure 6. (a) Images of piles for a CCGM with $d = 480\mu$m with increasing PBS coating; from left to right: no coating, slope= $27.7^o \pm 0.8$, $b = 52$nm slope=$40.3^o \pm 1.9$, $b = 62$ nm, slope = $42.5^o \pm 2.2$; (b) Dam break experiments of a cohesive material with $d = 0.8mm$ and $b = 200$nm. The three pictures illustrate the initial state, the onset of the flow and the final deposit.

[11] K. Kamrin, G. Koval, Phys. Rev. Lett. **108**, 178301 (2012)
[12] M. Bouzid, A. Izzet, M. Trulsson, E. Clément, P. Claudin, B. Andreotti, Eur. Phys. J E **38**, 1 (2015)
[13] P.G. Rognon, J.N. Roux, D. Wolf, M. Naaïm, F. Chevoir, Europhys. Lett. **74**, 644 (2006)
[14] P.G. Rognon, J.N. Roux, M. Naaim, F. Chevoir, J. Fluid Mech. **596**, 21 (2008)
[15] K. Johnson, K. Kendall, A.D. Roberts, Proc. R. Soc. A **324**, 301 (1971)
[16] S. Khamseh, J.N. Roux, F. Chevoir, Phys. Rev. E **92**, 022201 (2015)
[17] M. Badetti, A. Fall, F. Chevoir, P. Aimedieu, S. Rodts, J.N. Roux, J. Rheol **62**, 1175 (2018)
[18] N. Berger, E. Azéma, J. Douce, F. Radjai, Europhys. Lett. **112**, 64004 (2016)
[19] T.T. Vo, S. Nezamabadi, P. Mutabaruka, J.Y. Delenne, F. Radjai, Nat. Commun. **11**, 1 (2020)
[20] S. Mandal, M. Nicolas, O. Pouliquen, Proc. Natl. Acad. Sci. **117**, 8366 (2020)
[21] V. Richefeu, M.S. El Youssoufi, F. Radjai, Phys. Rev. E **73**, 051304 (2006)
[22] A.W. Alexander, B. Chaudhuri, A. Faqih, F.J. Muzzio, C. Davies, M.S. Tomassone, Powder Technol. **164**, 13 (2006)
[23] T.C. Halsey, A.J. Levine, Phys. Rev. Let. **80**, 3141 (1998)
[24] D.J. Hornbaker, R. Albert, I. Albert, A.L. Barabasi, P. Schiffer, Nature **387**, 765 (1997)
[25] R. Mani, D. Kadau, H.J. Herrmann, Granul. Matter **15**, 447 (2013)
[26] S. Mandal, D.V. Khakhar, Phys. Fluids **28**, 103301 (2016)
[27] L.E. Silbert, D. Ertaş, G.S. Grest, T. C.Halsey, D. Levine, S.J. Plimpton, Phys. Rev. E **64**, 051302 (2001)
[28] R. Brewster, G.S. Grest, J.W. Landry, A.J. Levine, Phys. Rev. E **72**, 061301 (2005)
[29] S. Bharathraj, V. Kumaran, Phys. Rev. E **97**, 012902 (2018)
[30] R. Wilson, D. Dini, B. van Wachem, AIChE J **62**, 1467 (2016)
[31] P. Liu, C.Q. LaMarche, K.M. Kellogg, C.M. Hrenya, Chem. Eng. Sci. **145**, 266 (2016)
[32] Y. Gu, S. Chialvo, S. Sundaresan, Phys. Rev. E **90**, 032206 (2014)
[33] B.V. Derjaguin, V.M. Muller, Y.P. Toporov, J. Colloid Interface Sci. **53**, 314 (1975)
[34] M. Macaulay, P. Rognon, Soft Matter (2020)
[35] P.D. Olmsted, Rheol. Acta **47**, 283 (2008)
[36] T. Divoux, M.A. Fardin, S. Manneville, S. Lerouge, Annu. Rev. Fluid Mech. **48**, 81 (2016)
[37] P. Coussot, J.S. Raynaud, F. Bertrand, P. Moucheront, J.P. Guilbaud, H.T. Huynh, S. Jarny, D. Lesueur, Phys. Rev. Lett. **88**, 218301 (2002)
[38] S.M. Fielding, Rep. Prog. Phys. **77**, 102601 (2014)
[39] E. Irani, P. Chaudhuri, C. Heussinger, Phys. Rev. Lett. **112**, 188303 (2014)
[40] E. Irani, P. Chaudhuri, C. Heussinger, Phys. Rev. E **94**, 052608 (2016)
[41] P. Chaudhuri, L. Berthier, L. Bocquet, Phys. Rev. E **85**, 021503 (2012)
[42] H. Perrin, C. Clavaud, M. Wyart, B. Metzger, Y. Forterre, Phys. Rev. X **9**, 031027 (2019)
[43] S. Luding, Granul. Matter **10**, 235 (2008)
[44] A. Gans, O. Pouliquen, M. Nicolas, Phys. Rev. E **101**, 032904 (2020)

[45] J. Modell, S. Thuresson, Patent **WO2008/020800A1** (2008)
[46] X. Li, D. Zhang, K. Xiang, G. Huang, RSC Adv. **4**, 32894 (2014)
[47] R. Albert, I. Albert, D. Hornbaker, P. Schiffer, A.L. Barabasi, Phys. Rev. E **56**, 6271 (1997)
[48] A. Samadani, A. Kudrolli, Phys. Rev. E **64**, 051301 (2001)
[49] S. Nowak, A. Samadani, A. Kudrolli, Nature **1**, 50 (2005)